ChemPubSoc Europe

DOI: 10.1002/ejic.201900904

EurJIC European Journal of Inorganic Chemistry

Full Paper

Anti-Parasitic Complexes

Organometallic Gold(III) Complexes with Tridentate Halogen-Substituted Thiosemicarbazones: Effects of Halogenation on Cytotoxicity and Anti-Parasitic Activity

Federico Salsi,[a] Gisele Bulhões Portapilla,[b] Konstantin Schutjajew,[a] Maximilian Roca Jungfer,[a] Amanda Goulart,[b] Adelheid Hagenbach,[a] Sérgio de Albuquerque,[b] and Ulrich Abram*[a]

Abstract: Chemical properties and biological activity of Au(III) compounds obtained from dichlorido[2-(dimethylaminomethyl)phenyl-C^1,N]gold(III), [Au(damp-C^1,N)Cl_2], and halogenated, potentially tridentate thiosemicarbazones have been studied. The results of this work show that the complexation of the halogenated thiosemicarbazones with Au(III) enhances their stability against hydrolysis and retains or enhances their anti-parasitic activity. Fluorination in the periphery of the ligands has expectedly no influence on the structural chemistry of the obtained Au(III) complexes, but modulates their biological behaviour. Best results with a remarkably high selectivity index for the trypomastigote form of *Trypanosoma cruzi* were obtained with the complex containing the ligand, which presents a 3,5-fluorine substitution in meta-position of an aromatic ring, [Au(dampH)(L-3,5-F)]Cl.

Introduction

American trypanosomiasis or Chaga's disease, caused by the parasite *Trypanosoma cruzi*, is a major public health problem in Latin America, where it constitutes one of the leading causes of mortality from cardiovascular diseases. Besides this, the problem is expanding to global proportions as a consequence of migration. Currently available chemotherapy of trypanosomiasis basing on a nitrofuran (nifurtimox) and a nitroimidazole (benznidazole) is unsatisfactory because of their poor efficacy in the chronic stage of the disease and severe side effects. Therefore, new approaches to specific chemotherapy are being developed.[1–3]

Gold(III) complexes acquire an important role in the research against parasitic diseases. The affinity of gold-based compounds for thiol- and selenol-containing proteins, which have been identified as drug targets in trypanosomes, makes them promising candidates in this field.[4] Recently, some gold(III)

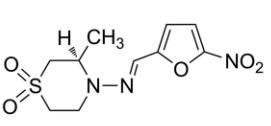

Nifurtimox

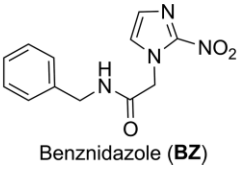

Benznidazole (**BZ**)

thiosemicarbazone (H_2tsc) complexes of the composition [Au(dampH)(tsc)]Cl derived from the organometallic precursor dichlorido[2-(dimethylaminomethyl)phenyl-C^1,N]gold(III), [Au(damp-C^1,N)Cl_2] were studied for their trypanocidal activity. *In vitro* biological assays showed reasonable cytotoxic and potent trypanocidal effects. The structure-activity relationship of a series of such compounds indicates that substituents at the thiosemicarbazone moiety have a significant effect on the biological activities of the complexes. The non-coordinated thiosemicarbazones show lower activity than their Au(III) complexes and the complexation also increases the stability of the molecules.[5] The high potential observed for these compounds, particularly those with $R^1 = R^2 = CH_3$, is the motivation for further investigations and optimization of their properties.

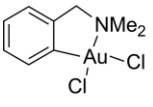

[AuCl$_2$(damp-C^1,N)]

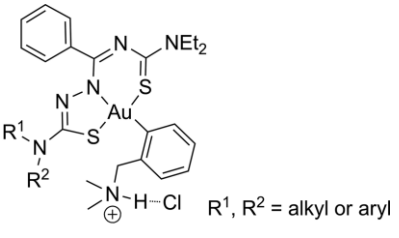

R^1, R^2 = alkyl or aryl

[Au(dampH)(tsc)]Cl

Fluorine-containing compounds play a central role in medicinal chemistry. It is known that the selective introduction of

[a] *Freie Universität Berlin, Institute of Chemistry and Biochemistry, Fabeckstr. 34–36, D-14195 Berlin, Germany*
E-mail: ulrich.abram@fu-berlin.de
URL: https://www.bcp.fu-berlin.de/chemie/chemie/forschung/InorgChem/agabram/index.html
[b] *Universidade de São Paulo, Faculdade de Ciências Farmacêuticas de Ribeirão Preto, Av. do Café – Vila Monte Alegre, Ribeirão Preto, SP, 14040-903, Brazil*
URL: http://fcfrp.usp.br/

Supporting information and ORCID(s) from the author(s) for this article are available on the WWW under https://doi.org/10.1002/ejic.201900904.

fluorine into an organic molecule can productively influence conformation, pK_a, intrinsic potency, membrane permeability, metabolic pathways, and pharmacokinetic properties. In the last fifty years, nearly 150 fluorinated molecules have been approved for therapeutic use. In 2010, it was calculated that about 20 % of administered drugs contain fluorine atoms or fluoroalkyl groups. This trend is increasing from 20 % to about 30 % for all new approved drugs, excluding biopharmaceutical products.[6] There is, in theory, no reason to expect that the positive effects induced by fluorine on the medical properties of organic pharmaceuticals might not be observed for metal complexes as well. Nevertheless, not many studies have been conducted in this field.[7,8]

Recently, we demonstrated that the fluorination of thiosemicarbazones can enhance their antiparasitic activity.[9] But at the same time an increased hydrolytic instability was observed, which complicates the comprehension of their mechanism of action. Thus, the question arises, whether the complexation of the fluorinated ligands can stabilize the molecule and improve the anti-*Trypanosoma cruzi* activity. Consequently, we synthetized halogenated analogues of the anti-trypanosomal compound obtained by Maia et al. ($R^1 = R^2 = CH_3$),[5] and studied how the halogen-substitution influences the hydrolytic and redox stability, the solubility and the anti-parasitic activity of the novel Au(III)-thiosemicarbazone complexes.

Results and Discussion

Reactions of [Au(damp)Cl_2] with the thiosemicarbazones of Scheme 1 give orange-red solids of the composition [Au(dampH)(L-X)]Cl. The products are soluble in common organic solvents like MeOH, CH_2Cl_2 or DMSO. They were characterized by elemental analysis, IR and multinuclear NMR spectroscopy, mass spectrometry, and some representatives by X-ray diffraction.

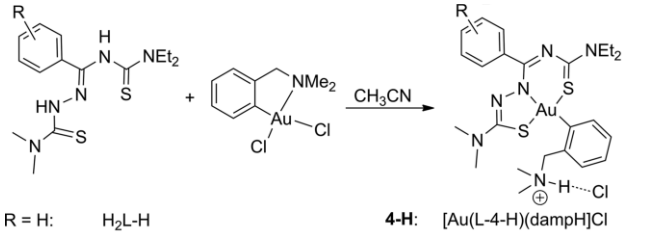

R = H: H_2L-H
R = 4-Cl: H_2L-4-Cl
R = 4-Br: H_2L-4-Br
R = 4-F: H_2L-4-F
R = 3-F: H_2L-3-F
R = 4-CF_3: H_2L-4-CF_3
R = 3-CF_3: H_2L-3-CF_3
R = 3,5-diF: H_2L-3,5-diF

4-H: [Au(L-4-H)(dampH]Cl
4-Cl: [Au(L-4-Cl)(dampH]Cl
4-Br: [Au(L-4-Br)(dampH]Cl
4-F: [Au(L-4-F)(dampH]Cl
3-F: [Au(L-3-F)(dampH]Cl
4-CF_3: [Au(L-4-CF_3)(dampH]Cl
3-CF_3: [Au(L-3-CF_3)(dampH]Cl
3,5-diF: [Au(L-3,5-diF)(dampH]Cl

Scheme 1. Synthesis of the Au(III) complexes.

The IR spectra of the compounds show broad bands around 3350 cm^{-1}, which can be assigned to the NH groups. This is in accordance with the protonation of the uncoordinated amino group of the dampH ligand. Sharp, very intense absorptions in the range between 1490 and 1495 cm^{-1} belong to the C=N stretches of the ligand.

The ^{1}H NMR spectra were recorded in $CDCl_3$. The NH signals of the thiosemicarbazones around 9.4 ppm disappear upon coordination confirming the double deprotonation of the ligands. New signals appear at low-field in the region between 12.2 and 12.3 ppm, corresponding to the protonated amino group of the dampH ligand. The aromatic range of the spectrum shows the resonances of the two substituted phenyl rings of the ligands between 8.12 and 6.80 ppm. The set of signals of the dampH ring is only weakly affected by the fluorine substitution and is similar in all compounds. The resonances of the thiosemicarbazone rings, however, are shifted and change in multiplicity, number and integral with respect to the fluorine substitution. For the para-substituted ligands, they can easily be identified by their integrals. For the meta-substituted ligands, the pattern becomes more complex and the signals can be assigned based on their multiplicity and by a comparative analysis of the spectra.

Two doublets of doublets are found at 4.4 and 4.5 ppm. They belong to the two non-equivalent geminal protons of the methylene groups of damp, which additionally couple to the NH protons with a coupling constant of ca. 13 Hz. The most plausible reason for the inequivalence of the CH_2 protons is given by steric constraints due to the relatively short Au–C bonds and the bulky dimethylammonium substituent (see also the space-filling model in Figure 1, which has been drawn using the van der Waals radii of the atoms).[10,11] The formation of agostic CH···Au interactions (Au···H distances between 2.742 and 2.771 Å) might not completely be ruled out, but are improbable in the light of a recent re-consideration of a large number of Au(I) and Au(II) complexes with relatively short Au···H distances.[12]

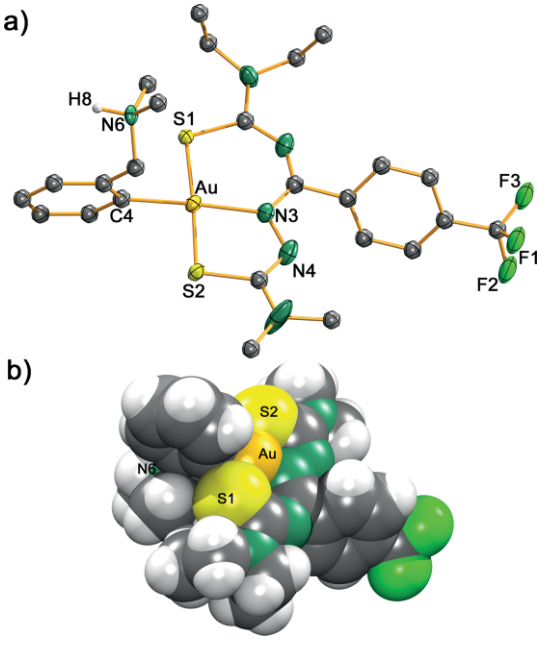

Figure 1. a) Ellipsoid plot of the complex cation of **4-CF_3** (thermal ellipsoids represent 50 % probability, hydrogen atoms bonded to carbon atoms have been omitted for clarity) and b) space-filling model with the van der Waals radii.

The ^{1}H NMR signals of the remaining alkyl protons are found in the region between 3.6 and 1.0 ppm. They are not split as a

consequence of a hindered rotation around the C-NEt_2 bonds, as is frequently observed for ligands and complexes of this type.[8,9] The methyl resonance appears as well-resolved triplet, while the methylene signals are broadened, probably due to the fact that the coalescence temperature of the system is near to room temperature.

The unambiguous assignment of the ^{13}C signals is possible by means of the ^{19}F-^{13}C couplings and comparison with the signals of related oxidorhenium(V) complexes, in which key positions of the ligands were ^{13}C-enriched. The signals of the imine carbon atoms are shifted up-field upon complex formation, while the C=S resonances are down-field shifted from the range between 178 and 182 ppm by about 20 ppm. Thus, the C=N signals are found right beside the more shielded C=S ones. This is clearly confirmed by the ^{13}C spectrum of compound **3,5-diF**, for which the signal at 154.1 ppm is a triplet, doubtlessly indicating the proximity of the related carbon atom to the two fluorine atoms in the meta positions of the phenyl ring.

All the ^{19}F NMR spectra present one signal, indicating the purity of the compounds. The signal of the mono-fluorinated complexes are slightly up-field shifted (ca. 2 ppm) in comparison to the uncoordinated ligands. The trifluoromethyl groups are not sensible to the complex formation.

All ESI^+ mass spectra show exclusively the molecular ions of the cationic complexes with high intensities. An additional peak, which is also observed in all spectra appears at m/z = 74.097 and can most probably be assigned to the elimination of $H_2NEt_2^+$ cations (calculated mass: 74.0969). There was no evidence for the formation of Au(I) species or hydrolysis products of the fluorinated ligands. Obviously, the fluorination does not affect the stability of the gold(III) damp complexes, which is unlike the behavior of related complexes of the composition [Au(L-X)Cl], where considerable cyclization of the thiosemicarbazones and the formation of Au(I) complexes was observed and unambiguously detected in the mass spectra of the complexes.[13]

The low solubility of the compounds in water prevents the use of ^{19}F NMR spectroscopy for the estimation of their stability in the aqueous medium used in the biological tests.

Single crystals suitable for X-ray diffraction could be grown for three gold complexes with fluorinated ligands (**4-F**, **4-CF_3** and **3-CF_3**). An ellipsoid representation of the structure of the complex cation of compound **4-CF_3** is depicted in Figure 1a. The structures of the other complexes are virtually identical (with the exception of the respective positions of fluorine atoms) and, thus, not shown here in extra Figures (but details are contained in the Supporting Information). Selected bond lengths and angles for the three compounds are given in Table 1. For comparison, the values for the non-fluorinated complex [Au(dampH)(L-H)]NO_3 (**4-H**) have been included.

The bond lengths and angles of Table 1 clearly show that the fluorination of the ligands has only minor influence on the molecular structures of the formed gold complexes. No significant differences in the bond lengths and angles are observed between the fluorinated complexes and the previously reported non-fluorinated compound [Au(dampH)(L-H)]NO_3.[5] The double-deprotonated thiosemicarbazones coordinate the gold

Table 1. Selected bond lengths [Å] and angles [°] for **4-CF_3**, **4-F** (two independent species), **3-CF_3** and the non-fluorinated complex [Au(dampH)(L-H)]-NO_3 (**4-H**).[a]

	4-H	4-CF_3	4-F·H_2O·0.5C_6H_6	3-CF_3
Au–S1	2.278(3)	2.281(2)	2.286(2), 2.284(3)	2.280(3)
Au–S2	2.281(3)	2.279(2)	2.284(3), 2.274(3)	2.279(3)
Au–N3	2.067(7)	2.046(5)	2.050(8), 2.057(8)	2.04(1)
Au–C4	2.039(9)	2.040(5)	2.04(1), 2.03(1)	2.020(9)
C3–S2	1.775(9)	1.767(7)	1.76(1), 1.77(1)	1.75(1)
C1–S1	1.77(1)	1.752(6)	1.76(1), 1.76(1)	1.75(1)
C4–Au–N3	175.5(2)	174.3(2)	174.7(3), 175.1(3)	174.8(4)
C4–Au–S1	86.2(3)	88.3(2)	87.8(3), 87.1(3)	89.5(3)
N3–Au–S1	97.8(2)	97.0(2)	97.5(3), 97.7(2)	96.5(3)
C4–Au–S2	91.4(3)	89.1(2)	90.0(3), 89.5(3)	89.1(2)
N3–Au–S2	84.5(2)	85.6(2)	84.7(2), 85.7(3)	86.0(3)
S1–Au–S2	177.5(2)	176.43(6)	176.2(1), 176.59(9)	175.8(1)

[a] Values for [Au(dampH)(L-H)]NO_3 are taken from ref.[5].

atoms as *S,N,S*-chelates. The fourth coordination position of the distorted square coordination sphere is occupied by the organometallic ligand. As in the non-fluorinated complexes,[5] the damp ligand coordinates monodentate and the nitrogen atom of the dimethylamino group is protonated. It forms a hydrogen bond to the Cl^- counterion.

Although the fluorination of the thiosemicarbazones has almost no influence on the molecular structures of the formed complexes and their stability, the packing patterns of the solid-state structures are strongly influenced by the introduction of the fluorine atoms or CF_3 groups. Figure 2 illustrates the crystal packing of **4-F**. Similarly to the situation in [Au(dampH)(L-H)]Cl,[5] the cations of **4-F** are arranged in double-layers with alternate polarity, which allows the co-crystallization of water and benzene in the same crystal. Two molecules are stacked to each other and face themselves across their non-polar sides forming hydrophobic pockets. They are filled with a benzene molecule. Between the two pairs of molecules is a hydrophilic space, to which the dimethylammonium groups point. This void is filled with the chloride ions and water molecules. There are hydrogen bonds between the dimethylammonium groups and the counterions and between Cl^- and the water molecules.

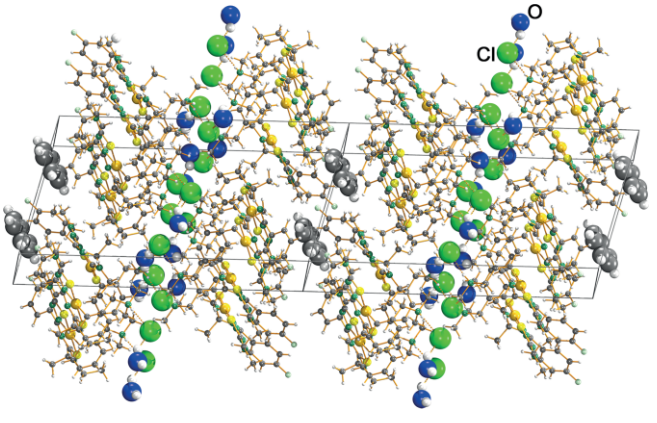

Figure 2. Crystal packing of **4-F** with co-crystallized benzene and water molecules.

The solid-state structure of the more lipophilic molecule **4-CF_3** has a more compact packing, which is dominated by lipo-

philic interactions. The molecules form parallel layers and the hydrophilic units point outward and interact with the counterions. As a result, orthogonal lipophilic and hydrophilic layers alternate each other. The trifluoromethyl group in the meta-position has a similar effect. It is noteworthy that the crystal packing of **3-CF_3** affords the proximity of the CF_3 groups, which probably enhances the stabilization of hydrophobic interactions (for a Figure see Supporting Information).

Recently, we reported the remarkable activity of seven halogen-substituted thiosemicarbazones against the flagellated protozoa *T. cruzi*.[9] The results encouraged us to continue the *in vitro* experiments with the gold(III) complexes of the present study, which contain the halogenated ligands of the previous work. The influence of the metal centers and halogen substituents were exploited on epimastigote, trypomastigote and amastigote forms of *T. cruzi*. The results are summarized in Table 2.

T. cruzi has a complex life cycle involving evolutive transformations in vertebrate (mammals) and invertebrate hosts (*Reduviidae* insect family).[14] Epimastigote forms live in the invertebrate host and are unable to establish mammalian infection.[15] Although non-infective to mammalian, the biological activity in these forms can provide knowledge about the structure-activity relationship, especially when a class of compounds may act in essential molecular targets for three evolutive forms of parasites, as discussed below.[16]

The percentages of growth inhibition in epimastigotes are given in terms of IC_{50} values and compared to the reference drug benznidazole (**BZ**). Almost all Au(III) complexes of this study show a high activity at low micromolar concentrations and they are statistically as active as **BZ**. An exception is complex **4-Cl**, which contains a chlorine substituent. Interestingly, the presence of chlorine seems to diminish drastically the biological activity of the thiosemicarbazone complex, what is evidenced by the lack of epimastigotes inhibition even at the maximum concentration tested (IC_{50}>100 μM).

Although Au(III) and Pt(II) ions are isoelectronic and their complexes are frequently isostructural, it is not very probable that the mechanism of the biological activity of the complexes under study is DNA-related as is known for the anti-cancer activity of compounds of the cis-platin family.[17] Gold(III) compounds frequently trigger other biochemical mechanisms by modification or selective inhibition of thiol- or selenol-containing proteins.[4,17,18] Recent studies have shown that thiosemicarbazones may inhibit cruzain, the major thiol-containing enzyme from *T. cruzi*, by attaching irreversibly to the catalytic Cys25 thiol group of this compound.[19,20] Expressed in all stages of the *T. cruzi* life cycle, cruzain is essential to many biological processes including metacyclogenesis (invertebrate stage) and host invasion and evasion of the host immune response (vertebrate stage) by the parasite.[17]

The presence of a large number of trypomastigote forms in the bloodstream marks the acute phase of Chagas disease in mammalian hosts and all types of nucleated cells in the hosts are potential targets for infection.[21] A serial dilution of the Au(III) complexes was performed to determine the concentrations, which kill 50 % of trypomastigotes ($IC_{50\ tryp}$). All halogenated compounds show a high activity at very low concentrations. The $IC_{50\ tryp}$ values of the complexes with the fluorinated ligands are approximately five times lower than that of benznidazole. Only the activity of **4-H, 4-Br** and **3-F** and **4-Cl** is somewhat lower, but still in the range of **BZ** or better. It is remarkable that trypomastigotes appear to be much more susceptible to **4-Cl** than the epimastigote forms of the parasite.

Lopes and co-workers showed the effective activity of the non-halogenated [Au(dampH)(L-H)]Cl.[22] It eliminates both the extracellular trypomastigote and the intracellular amastigote forms of the parasite. In very-low-dose *in vivo* assays, the gold complex also reduced blood parasitaemia and tissue parasitism in the acute phase of Chagas disease. It is well-known that trypomastigotes play an important role during the progression to the chronic phase of Chagas disease.[23] In immunocompetent patients, the acute phase is controlled by the effector action of the immune response, but it cannot completely eliminate the blood parasites that migrate easily to target tissues where they invade cells and transform into proliferative amastigote forms.[24] In this sense, the efficacy of the metal compounds was also investigated on the intracellular stage of *T. cruzi* after infection of LLC-MK2 cells.

An increase in LLC-MK2 cells survival and amastigotes proliferation inhibition presents a measure of the effectiveness of potential drugs. In contrast, the death of the host cells during the analyses is indicative of cytotoxicity. In this sense, the ratio between the cytotoxic activity (CC_{50}) and trypanocidal activity (IC_{50}) is also provided in Table 2, in order to determine the

Table 2. Activity of the Au(III) complexes against *T. cruzi* in different life stages of the parasite and cytotoxicity in mammalian cells.[a]

Compound	epimastigotes IC_{50} ± SD	trypomastigotes IC_{50} ± SD	amastigotes IC_{50} ± SD	LLC-MK2 CC_{50} ± SD	SI $CC_{50}/IC_{50\ tryp}$	SI $CC_{50}/IC_{50\ ama}$
4-H	24.7 ± 7.0	8.4 ± 2.4	9.2 ± 1.2	23.8 ± 1.3	2.8	2.6
4-Cl	> 100	18.0 ± 3.8	>100	99.0 ± 1.3	5.5	ND
4-Br	14.1 ± 4.8	5.7 ± 1.9	56.0 ± 2.4	96.8 ± 5.6	16.9	1.7
4-F	11.1 ± 2.9	3.9 ± 0.5	27.2 ± 1.3	46.4 ± 6.5	11.9	1.7
3-F	12.3 ± 0.3	8.7 ± 1.0	28.2 ± 6.8	61.7 ± 8.4	7.1	2.2
4-CF_3	8.4 ± 0.6	4.0 ± 0.6	33.8 ± 2.7	66.5 ± 6.2	16.7	2.0
3-CF_3	16.0 ± 3.6	3.6 ± 0.6	23.4 ± 5.9	65.4 ± 3.6	18.2	2.8
3,5-diF	8.9 ± 1.2	3.2 ± 0.4	19.3 ± 2.5	60.6 ± 6.6	18.8	3.1
BZ	14.3 ± 3.0	15.7 ± 3.4	5.0 ± 0.5	> 100	>6.4	>20.2

[a] Values of concentration are represented in μM. IC_{50}, Mean values ± SD of three independent experiments. SI: selectivity index from ratio of CC_{50} to IC_{50}. **BZ**: Benznidazole. ND: not determined.

selectivity index for the individual gold complexes (SI = CC_{50}/IC_{50}).[25]

The gold complexes do not inhibit the proliferation of amastigotes in concentration equal or smaller than that of **BZ**. Except for **4-Br,** the coordination of the thiosemicarbazones to gold appears to increase the toxicity of the compounds when compared to the non-coordinated compounds. This effect is independent of the halogen-substitution. Interestingly, the Cl- and Br-substituted complexes show a lower trypanocidal activity than the respective non-coordinated thiosemicarbazones.

The differences in trypanocidal activity and cytotoxicity between the non-coordinated thiosemicarbazones and their gold chelates is not unexpected with regard to the changes in polarity, charge and solubility of the respective compounds. The increased lipophilicity after complexation enhances their cellular uptake, but also decreases their solubility in aqueous media, which is a serious drawback in terms of bioavailability,[26] and can in worst case distort the obtained *in vitro* results. We came across such an effect when we re-evaluated some of the previously determined *in vitro* parameters of the non-halogenated complex **4-H**.[22] Actually, we found that the previously determined CC_{50} value for this compound was too high, most probably due to an insufficient solubility at higher concentrations. Thus, the values of Table 2 shall be used for comparison with the data of the halogenated complexes.

In fact, the improved anti-*T. cruzi* activity, which has been found for the halogenated thiosemicarbazones when compared to their non-halogenated representative,[9] can also be confirmed for their gold(III) chelates. Here, it was demonstrated that Au complexes may also act effectively in the control of trypomastigotes in low concentrations. Expanding the relation between cytotoxicity and anti-trypomastigote activity, the selectivity index was provided. Except **4-Cl** and **3-F**, all the complexes possess SI's higher than 10, which recommends them to anti-*T. cruzi* assays. Compound **3,5-diF** gives the best biological effects on epimastigote (IC_{50} 8.9 ± 1.2 μM), trypomastigote (IC_{50}= 3.2 ± 0.4 μM, SI = 18.8) and amastigote (19.3 ± 2.5 μM, SI = 3.1) forms of *T. cruzi*.

Conclusions

A series of organometallic Au(III) complexes with halogenated thiosemicarbazone ligands were prepared and completely characterized. Three of them were also studied by single-crystal X-ray diffraction, showing that the fluorination has only minor influence on the molecular structures of the complexes, but strongly influence their solid-state structures. Unlike the uncoordinated thiosemicarbazones,[9] the gold complexes are stable at room temperature as solids and in solution, Thus, the coordination with the {Au(dampH)} moiety is a convenient tool, for stabilizing the halogenated ligands, maintaining and, in some cases, even enhancing their biological activity.

The possibility to modulate lipophilicity, pharmacokinetic properties and bioavailability of potential drugs by halogen-substitution has previously been demonstrated for a series of halogenated thiosemicarbazones.[9,27] The main problem with these compounds, their low stability as solids, could be solved by the preparation of stable gold(III) chelates. The halogen-substituted Au(III) complexes are highly active in trypomastigote forms of *T. cruzi*. The results of the present study encourage to perform ongoing studies, mainly dealing with *in vivo* low dose protocols, which may provide deeper knowledge about biodistribution, biotransformation and pharmacokinetic parameters and give us more clinically-relevant information on the design of new anti-trypanosomiasis drugs on the basis of such complexes for clinical studies.

Another interesting result of the present study is the higher cytotoxicity of the gold complexes to LLC-MK2 cells compared to the uncoordinated ligands, and the lower activity against amastigote forms (intracellular form) than against trypomastigote forms (extracellular). From this, it may be concluded that these compounds shall also be cytotoxic against cancer cells. The effectiveness of gold compounds in biological systems depends on a series of complex interactions between metals, cellular components and genes. However, not different from other compound classes, they can also induce deleterious effects on healthy cells. Considering the different mechanisms of action that gold compounds may have *(vide supra)*, future studies should be encouraged to investigate the antiparasitic mechanism of action of these complexes as well as to investigate them for anti-cancer activity.

Experimental Section

Materials and methods. [Au(damp)Cl_2] and the thiosemicarbazone ligands were prepared according to literature methods.[9,28] All other chemicals were purchased and used without further purification. NMR spectra were recorded with a JEOL 400 MHz multinuclear spectrometer. Positive and negative ESI mass spectra were measured with an Agilent 6210 ESI-TOF (Agilent Technology) mass spectrometer. Elemental analysis of carbon, hydrogen, nitrogen and sulfur were performed using a Heraeus elemental analyzer. Infrared spectra were recorded at an ATR-spectrometer (Nicolet iS10, Thermo Scientific).

X-ray crystallography. The intensities for the X-ray diffraction studies were collected on a Bruker D8 Venture or a STOE IPDS 2T instrument with Mo Kα radiation. Absorption corrections were carried out by SADABS or X-RED 32.[29,30] Structure solution and refinement were performed with the SHELX program package.[31,32] Hydrogen atoms were placed at calculated positions and treated with the "riding model" option of SHELXL. The representation of molecular structures was done using the program DIAMOND (vers. 4.5.1).[33]

CCDC 1947212 (for **4-CF_3**), 197213 (for **4-F**), and 1947214 (for **3-CF_3**) contain the supplementary crystallographic data for this paper. These data can be obtained free of charge from The Cambridge Crystallographic Data Centre.

Synthesis

General procedure for the synthesis of the [Au(dampH)(L-X)]Cl complexes. [Au(damp)Cl_2] (40 mg, 0.1 mmol) was dissolved in 2 mL of acetonitrile and H_2L (0.1 mmol) was added. The resulting orange-red solution was stirred overnight at room temperature. The addition of diethyl ether (5 mL) gave an orange-red solid, which was filtered off and dried in vacuo.

[Au(dampH)(L-4-Cl)]Cl (4-Cl): Orange-red solid (yield: quantitative). ^{1}H NMR ($CDCl_3$, ppm): δ = 12.34 (broad s, 1H, N-H), 8.10 (m, 1H, Ph-

damp), 7.61 (m, 2H, Ph-tsc), 7.47 (m, 3H, Ph-damp and Ph-tsc), 7.32 (m, 1H, Ph-damp), 7.22 (m, 1H, Ph-damp), 4.46 (two broad m, 2H, Ar-CH_2N^+H), 3.64 (broad m, 4H, CH_2CH_3), 2.97 (s, 6H, N^+H-CH_3), 2.80 (d, 6H, J = 4.7 Hz, NCH_3), 1.18 (t, 6H, J = 6.9 Hz, CH_2CH_3). ^{13}C NMR ($CDCl_3$, ppm): δ = 162.1 (s, C=S), 154.2 (s, C=S), 153.9 (s, C=N), 135.7 (s, C-Cl), 135.4 (s, Ph-damp), 133.8 (s, Ph-damp), 132.1 (s, Ph-damp), 131.3 (s, Ph-damp), 131.2 (s, C quat. Ph-tsc), 130.3 (s, Ph-tsc), 129.3 (s, Ph-damp), 127.0 (s, Ph-damp), 126.4 (s, Ph-tsc), 62.7 (s, Ar-CH_2N^+H), 42.4 and 41.8 (two s, CH_2CH_3 and N^+H-CH_3), 40.7 (s, N-CH_3), 12.0 (s, CH_2CH_3). IR (cm^{-1}): $\tilde{\nu}$ = 3365 m (NH), 2975 w, 2935 m, 2795 w, 2618 m, 2470 m, 1584 w, 1553 m, 1487 vs. (C=N), 1449 vs, 1430 s, 1415 vs, 1366 s, 1345 vs, 1300 m, 1291 m, 1262 m, 1243 m, 1207 m, 1176 w, 1148 m, 1134 m, 1098 m, 1086 s, 1075 s, 1051 m, 1027 m, 1012 s, 949 m, 918 s, 869 m, 838 s, 811 w, 788 w, 762 s, 726 m, 714 m, 680 w, 658 w, 643 w, 625 w, 607 w, 594 w, 581 m, 564 w, 530 w. Elemental analysis: Calcd for $C_{24}H_{34}AuCl_2N_6S_2{\cdot}H_2O$: C 38.1, H 4.7, N 11.1, S 8.5; found C 36.9, H 4.6, N 10.3, S 9.8 %. ESI MS (m/z): $[M]^+$ 701.1572 (calcd for $C_{24}H_{33}AuClN_6S_2$: 701.1557).

[Au(dampH)(L-4-Br)]Cl (4-Br): Orange-red solid (yield: 92 %). ^1H NMR ($CDCl_3$, ppm): δ = 12.38 (broad s, 1H, N-H), 8.10 (dd, J = 7.7 Hz, 1.2 Hz, 1H, Ph-damp), 7.69 (m, 2H, Ph-tsc), 7.48 (dd, J = 7.8, 1.2 Hz, 1H, Ph-damp), 7.35–7.30 (two m, 3H, Ph-tsc and Ph-damp), 7.45 (td, J = 7.5, 1.4 Hz, 1H, Ph-damp), 4.53–4.40 (two dd, 1H, J = 13.3, 5.7 Hz, Ar-CH_2-N^+H), 3.65 (br, 4H, CH_2CH_3), 2.98 (s, 6H, N-CH_3), 2.82 (d, 6H, J = 4.7 Hz, N^+H-CH_3), 2.78 (d, 6H, J = 4.7 Hz, N^+H-CH_3), 1.19 (t, 6H, J = 6.9 Hz, CH_2CH_3). ^{13}C NMR ($CDCl_3$, ppm): δ = 163.1 (s, C=S), 155.3 (s, C=S), 154.8 (s, C=N), 137.3 (s, C-Br), 136.4 (s, Ph-damp), 133.1 (s, Ph-damp), 132.3 (s, Ph-damp), 132.4 (s, Ph-damp), 131.6 (s, Ph-tsc), 130.4 (s, Ph-tsc), 130.3 (s, Ph-damp), 128.0 (s, damp), 123.2 (s, quat. Ph-tsc), 63.7 (s, Ar-CH_2N^+H), 43.4 and 42.8 (two s, CH_2CH_3 and N^+H-CH_3), 41.7 (s, N-CH_3), 13.0 (s, CH_2CH_3). IR (cm^{-1}): $\tilde{\nu}$ = 3365 w (NH), 2976 w, 2936 w, 2795 w, 2562 w, 1583 w, 1522 m, 1495 vs. (C=N), 1449 vs, 1430 w, 1417 vs, 1387 w, 1365 m, 1346 vs, 1300 w, 1291 w, 1264 w, 1243 m, 1206 m, 1177 w, 1148 m, 1135 m, 1107 w, 1097 m, 1073 m, 1051 w, 1027 w, 1009 s, 949 m, 918 s, 870 m, 836 s, 811 w, 788 w, 763 s, 724 m, 702 w, 676 w, 658 w, 643 w, 608 w, 573 m, 562 w, 536 w. Elemental analysis: Calcd for $C_{24}H_{33}AuBrClN_6S_2{\cdot}H_2O$: C 36.0, H 4.4, N 10.5, S 8.0; found C 35.2, H 4.7, N 10.3, S 9.4 %. ESI MS (m/z): $[M]^+$ 745.1062 (calcd for $C_{24}H_{33}AuBrN_6S_2$: 745.1052).

[Au(dampH)(L-4-F)]Cl (4-F): Orange-red solid (yield: 54 %). ^1H NMR ($CDCl_3$, ppm): δ = 12.20 (broad s, 1H, N^+H), 8.08 (dd, J = 7.8, 1.5 Hz, 1H, Ph-damp), 7.75 (m, 2H, Ph-tsc), 7.47 (dd, J = 7.8, 1.2 Hz, 1H, Ph-damp), 7.31 (td, J = 7.5, 1.3 Hz, 1H, Ph-damp), 7.22 (td, J = 7.6, 1.5 Hz, 1H, Ph-damp), 7.02 (m, 2H, Ph-tsc), 4.46 (two dd, J = 13.4, 5.7 Hz, 2H, N^+H-CH_2-Ar), 3.64 (broad m, 4H, CH_2CH_3), 2.98 (s, 6H, N-CH_3), 2.80 (two d, J = 4.7 Hz, 6H, N^+H-CH_3), 1.18 (t, J = 6.9 Hz, 6H, CH_2CH_3). ^{13}C NMR ($CDCl_3$, ppm): δ = 163.1 (s, C=S), 163.0 (d, J = 248.7 Hz, C-F), 155.4 (s, C=S), 154.8 (s, C=N), 136.3 (s, Ph-damp), 133.9 (d, J = 3.4 Hz, C quat. Ph-tsc), 133.1 (s, Ph-damp), 132.2 (s, Ph-damp), 132.1 (s, Ph-damp), 132.0 (d, J = 8.2 Hz, Ph-tsc), 130.3 (s, Ph-damp), 128.0 (s, Ph-damp), 114.1 (d, J = 21.5 Hz, Ph-tsc), 63.7 (s, Ar-CH_2N^+H), 43.4 and 42.8 (two s, CH_2CH_3 and N^+H-CH_3), 41.7 (s, N-CH_3), 13.0 (s, CH_2CH_3). ^{19}F NMR ($CDCl_3$, ppm): –111.4 (m). IR (cm^{-1}): $\tilde{\nu}$ = 3343 w (NH), 2974 w, 2931 w, 2649 w, 1600 w, 1555 w, 1492 s (C=N), 1452 m, 1417 s, 1347 m, 1245 w, 1218 m, 1164 m, 1153 m, 1095 m, 1076 m, 948 m, 918 s, 837 s, 762 s, 728 w, 617 s. Elemental analysis: Calcd for $C_{24}H_{33}AuClFN_6S_2$: C 39.9, N 11.6, H 4.6, S 8.9; found C 39.1, N 11.1, H 4.7, S 8.4. ESI MS (m/z): $[M]^+$ 685.1849 (calcd for $C_{24}H_{33}AuFN_6S_2$: 685.1850).

[Au(dampH)(L-3-F)]Cl (3-F): Orange-red solid (yield: quantitative). Crystals suitable for X-ray crystallography were obtained by slow evaporation of a $CHCl_3$/benzene (v/v: 1:1) solution. ^1H NMR ($CDCl_3$, ppm): δ = 12.38 (broad s, 1H, N-H), 8.12 (broad m, 1H, Ph-damp), 7.42 and 7.52 (m, 3H, Ph-damp and Ph-tsc), 7.36 and 7.28 (m, 2H, Ph-damp and Ph-tsc), 7.24 (broad m, 1H, Ph-damp), 7.05 (m, 1H, Ph-tsc), 4.47 (dd, 1H, J = 13.3, 5.7 Hz, N^+H-CH_2-Ar), 4.38 (dd, 1H, J = 13.3, 5.7 Hz, N^+H-CH_2-Ar), 3.65 (br, 4H, CH_2CH_3), 2.98 (s, 6H, N-CH_3), 2.81 (d, 6H, J = 4.4 Hz, N^+H-CH_3), 2.73 (d, 6H, J = 4.4 Hz, N^+H-CH_3), 1.20 (t, 6H, J = 6.9 Hz, CH_2CH_3). ^{13}C NMR ($CDCl_3$, ppm): δ = 163.3 (s, C=S), 161.8 (d, J = 244.5 Hz, C-F), 155.0 (s, C=S), 155.0 (s, C=N), 140.3 (d, J = 7.8 Hz, quart. C, Ph-tsc), 136.3 (s, Ph-damp), 133.1 (s, Ph-damp), 132.2 (s, Ph-damp), 132.1 (s, Ph-damp), 130.3 (s, Ph-damp), 128.6 (d, J = 8.0 Hz, Ph), 128.0 (s, Ph-damp), 125.4 (d, J = 3.0 Hz, Ph-L), 116.8 (d, J = 23.3 Hz, Ph-tsc), 115.8 (d, J = 21.1 Hz, Ph-tsc), 63.6 (s, Ar-CH_2N^+H), 43.4 and 42.8 (two s, CH_2CH_3 and N^+H-CH_3), 41.7 (s, N-CH3), 12.9 (s, CH_2CH_3). ^{19}F NMR ($CDCl_3$, ppm): –114.7 (m). IR (cm^{-1}): $\tilde{\nu}$ = 3558 m (NH), 2974 w, 2933 w, 2872 w, 2795 w, 2619 w, 2474 w, 1637 w, 1612 w, 1584 m, 1556 m, 1489 vs (C=N), 1451 vs, 1415 vs, 1365 s, 1347 vs, 1300 m, 1267 m, 1252 m, 1222 s, 1189 w, 1130 s, 1108 m, 1092 m, 1074 m, 1052 m, 1027 w, 1011 w, 1001 w, 948 s, 902 s, 872 w, 861 m, 839 w, 785 w, 761 s, 723 w, 708 m, 690 w, 669 m, 653 m, 642 m, 607 w, 593 w, 566 m, 549 w, 535 w, 526 w. Elemental analysis: Calcd for $C_{24}H_{33}AuFClN_6S_2{\cdot}H_2O$: C 39.9, H 4.6, N 11.6, S 9.3; found C 37.9, H 5.1, N 11.0, S 8.8. ESI MS (m/z): $[M]^+$ 685.1867 (calcd for $C_{24}H_{33}AuFN_6S_2$: 685.1869).

[Au(dampH)(L-4-CF_3)]Cl (4-CF_3): Orange-red solid (yield: 56 %). ^1H NMR ($CDCl_3$, ppm): δ = 12.36 (broad s, 1H, N^+H), 8.10 (dd, J = 7.7, 1.4 Hz, 1H, Ph-damp), 7.79 (d, J = 8.1 Hz, 2H, Ph-tsc), 7.60 (d, J = 8.1 Hz, 2H, Ph-tsc), 7.49 (dd, J = 7.8, 1.2 Hz, Ph-damp), 7.33 (td, J = 7.6, 1.1 Hz, Ph-damp), 7.23 (td, J = 7.5, 1.5 Hz, Ph-damp), 4.55–4.39 (two m, N^+H-CH_2-Ar), 3.64 (4H, broad m, CH_2CH_3), 2.95 (s, 6H, N^+H-CH_3), 2.81 (2 broad m, 6H, N^+H-CH_3), 1.19 (t, J = 7.1 Hz, 6H, CH_2CH_3). ^{13}C NMR ($CDCl_3$, ppm): δ = 163.3 (s, C=S), 155.1 and 155.0 (two s, C=S and C=N), 142.3 (s, Ph-tsc), 136.3 (s, Ph-damp), 133.1 (s, Ph-damp), 132.3 (two s, Ph-damp), 130.4 (q, J = 32.4 Hz, Ph-tsc), 130.4 (s, Ph-damp), 129.7 (two s, Ph-tsc), 128.0 (s, Ph-damp), 124.2 (q, J = 172.3 Hz, C-F), 124.2 (q, J = 3.9 Hz, Ph-tsc), 63.7 (s, Ar-CH_2N^+H), 43.5 and 42.5 (broad, N^+H-CH_3 and CH_2CH_3), 41.6 (s, N-CH_3), 12.9 (s, CH_2CH_3). ^{19}F NMR ($CDCl_3$, ppm): –62.57 (s). IR (cm^{-1}): $\tilde{\nu}$ = 3360 w (NH), 2974 w, 2936 w, 2649 w, 1556 w, 1494 s (C=N), 1451 m, 1419 s, 1346 m, 1327 s, 1246 w, 1218 m, 1167 m, 1106 m, 1065 m, 920 m, 850 m, 763 m, 724 w, 574 m. Elemental analysis: Calcd for $C_{25}H_{33}AuClF_3N_6S_2$: C 38.9, N 10.9, H 4.3, S 8.3; found C 38.0, N 10.6, H 4.3, S 8.3. ESI MS (m/z): $[M]^+$ 735.1815 (calcd for $C_{25}H_{33}AuF_3N_6S_2$: 735.1820).

[Au(dampH)(L-3-CF_3)]Cl (3-CF_3): Orange-red solid (yield: 71 %). ^1H NMR ($CDCl_3$, ppm): δ = 12.32 (broad s, 1H, N-H), 8.11 (dd, J = 7.7, 1.5 Hz, 1H, Ph-damp), 8.08 (m, 1H, Ph-tsc), 7.92 (m, 1H, Ph-tsc), 7.60 (m, 1H, Ph-tsc), 7.51 and 7.45 (two m, 2H, Ph-damp and Ph-tsc), 7.33 (td, J = 7.6, 1.3 Hz, 1H, Ph-damp), 7.23 (td, J = 7.6, 1.5 Hz, 1H, Ph-damp), 4.51 (dd, 1H, J = 13.4, 5.7 Hz, Ar-CH_2N^+H), 4.43 (dd, 1H, J = 13.4, 5.7 Hz, Ar-CH_2N^+H), 4.43 (dd, 1H, J = 13.4, 5.7 Hz, Ar-CH_2N^+H), 3.65 (broad m, 4H, CH_2CH_3), 2.97 (s, 6H, N-CH_3), 2.83 (d, 6H, J = 4.9 Hz, N^+H-CH_3), 2.75 (d, 6H, J = 4.9 Hz, N^+H-CH_3), 1.20 (t, 6H, J = 7.0 Hz, CH_2CH_3). ^{13}C NMR ($CDCl_3$, ppm): δ = 163.4 (s, C=S), 155.0 (s, C=S), 154.5 (s, C=N), 139.1 (s, Ph-tsc), 136.3 (s, Ph-damp), 133.1 (s, Ph-damp), 132.9 (s, Ph-tsc), 132.3 (s, Ph-damp), 132.2 (s, Ph-damp), 130.4 (s, Ph-damp), 129.4 (q, J = 32.4 Hz, C-CF_3), 128.0 (s, Ph-tsc), 127.8 (s, Ph-damp), 127.3 (q, J = 3.9 Hz, Ph-tsc), 125.5 (q, J = 3.8 Hz, Ph-tsc), 124.3 (q, J = 272.3 Hz, CF_3), 63.7 (s, Ar-CH_2N^+H), 43.4 and 42.8 (two s, CH_2CH_3 and N^+H-CH_3), 41.6 (s, N-CH_3), 12.93 (s, CH_2CH_3). ^{19}F NMR ($CDCl_3$, ppm): –62.54 (s). IR (cm^{-1}): $\tilde{\nu}$ = 3366 m (NH), 2974 m, 2937 m, 2798 w, 2620 m, 2475 m, 1614 w, 1583 w, 1557 m, 1490 vs (C=N), 1452 vs, 1416 vs, 1370 s, 1333 vs, 1314 s, 1299 m, 1278 s, 1243 m, 1206 s, 1166 s, 1149 s, 1131 s, 1118 s, 1107

s, 1091 s, 1068 vs, 1051 s, 1027 m, 1011 m, 1000 m, 948 s, 925 m, 896 m, 877 m, 858 m, 839 w, 808 m, 788 m, 763 s, 723 w, 712 w, 704 m, 689 s, 670 s, 659 m, 645 m, 607 w, 593 w, 568 m, 549 w, 538 w. Elemental analysis: Calcd for $C_{25}H_{33}AuF_3ClN_6S_2$: C 38.9, H 4.3, N 10.9, S 8.7; found C 37.3, H 4.6, N 10.2, S 9.0. ESI MS (*m/z*): $[M]^+$ 735.1833 (calcd for $C_{25}H_{33}AuF_3N_6S_2$: 735.1837).

[Au(dampH)(L-3,5-diF)]Cl (3,5-diF): Orange-red solid (yield: 54 %). ^{1}H NMR ($CDCl_3$, ppm): δ = 12.26 (broad s, 1H, N^+H), 8.12 (dd, *J* = 7.7, 1.5 Hz, 1H, Ph-damp), 7.46 (dd, *J* = 7.8, 1.2 Hz, 1H, Ph-damp), 7.32 (td, *J* = 7.5, 1.3 Hz, 1H, Ph-damp), 7.25 and 7.20 (m, 3H, Ph-damp and tsc), 6.81 (tt, *J* = 8.8, 2.3 Hz, 1H, Ph-tsc), 4.46 (two dd, *J* = 13.4, 5.6 Hz, 2H, N-CH_2-Ph), 3.64 (s, 3H, CH_2CH_3), 3.05 (s, 6H, N-CH_3), 2.82 (two d, *J* = 4.6 Hz, 6H, N-CH_3), 1.21 (t, *J* = 7.0 Hz, 6H, CH_2CH_3). ^{13}C NMR ($CDCl_3$, ppm): δ = 164.6 (s, C=S), 162.3 (dd, *J* = 247.5, 12.4 Hz, C-F), 155.8 (s, C=S), 154.1 (t, *J* = 2.9 Hz, C=N), 141.0 (t, *J* = 9.6 Hz, quat. Ph-tsc), 136.1 (s, Ph-damp), 133.0 (s, Ph-damp), 132.4 (s, Ph-damp), 131.5 (s, Ph-damp), 130.4 (s, Ph-damp), 128.1 (s, Ph-damp), 112.8 (m, Ph-tsc), 104.5 (t, *J* = 25.4 Hz, Ph-tsc), 63.5 (s, Ar-CH_2N^+H), 43.3 and 42.8 (two s, CH_2CH_3 and N^+H-CH_3), 42.0 (s, N-CH_3), 12.9 (CH_2CH_3). ^{19}F NMR ($CDCl_3$, ppm): –110.77 (broad m). IR (cm^{-1}): $\tilde{\nu}$ = 3351 w (NH), 2972 w, 2935 w, 2647 w, 1622 w, 1598 w, 1554 w, 1494 s (C=N), 1417 s, 1348 s, 1277 m, 1238 m, 1118 s, 1075 m, 988 s, 947 m, 907 s, 846 m, 760 m, 739 m, 723 w, 711 m, 658 m, 568 m. Elemental analysis: Calcd for $C_{24}H_{32}AuClF_2N_6S_2$: N 11.3, C 39.0, S 8.6, H 4.36; found N 11.0, C 37.7, S 8.3, H 4.3. ESI MS (*m/z*): $[M]^+$ 703.1754 (calcd for $C_{24}H_{32}AuF_2N_6S_2$: 703.1760).

Biological Tests

Parasites, mammalian cells and compounds. The experiments were performed using the Tulahuen strain of *T. cruzi* transfected with the *Escherichia coli* β-galactosidase gene lacZ.[34] Epimastigote forms were cultivated at 28 °C in liver infusion tryptose (LIT) medium,[35] continuously maintained in logarithmic growth by weekly passages. Trypomastigote forms were maintained by weekly inoculations in monkey kidney cells LLC-MK2 (ATCC® CCL-7™) cultivated in RPMI-1640 medium (Roswell Park Memorial Institute – Sigma-Aldrich) at 37 °C in humidified air and 5 % CO_2. Both media were supplemented with 10 % fetal bovine serum (FBS), 50 U/mL penicillin, 0.05 mg/mL streptomycin. The compounds were dissolved in dimethyl sulfoxide and used at a concentration of less than 1 % during experiments. Benznidazole (BZ) (Sigma-Aldrich) was used as positive control.

Epimastigotes growth inhibition assay. The activity of the gold complexes against epimastigotes was assessed by the fluorescence resazurin assay as described previously.[36] In a 96-well microplate, epimastigotes in log-phase were seeded at 1×10^6 epimastigotes/well with different concentrations (100–0.78 μM) of the Au complexes and BZ in duplicate. After 72 h at 28 °C, parasites viability was assessed by adding 10 μL/well of resazurin solution (0.1 %), followed by incubation for 5 h at 37 °C. Fluorescence intensity was measured using a microplate reader (Synergy H1 Biotek) at $\lambda_{excitation}$ of 530 nm and at $\lambda_{emission}$ of 600 nm. The inhibitory concentration that reduces 50 % of parasites viability (IC_{50}) was calculated by a dose-response curve regarding the untreated control.

Trypomastigotes inhibition assay. Trypomastigotes were harvested from the supernatant of LLC-MK2 cells six days post infection *in vitro*. Parasites were centrifuged at 1000 rpm for 10 min to remove dead cells. Remaining supernatant was centrifuged at 3000 rpm for 10 min and concentration was adjusted at 5×10^5 parasites/well in fresh RPMI medium. Trypomastigotes were incubated in 96-well plates with different concentrations (100–0.78 μM) of the Au complexes and BZ in duplicate. After incubation for 24 h at 37 °C, the 50 % effective concentrations (EC_{50}) of the compounds were obtained regarding untreated control afterward counting mobile parasites in an optic microscope.[37]

Intracellular amastigotes inhibition assay. LLC-MK2 cells were cultivated in 96-well plates (5×10^3 cells/well) with Tulahuen trypomastigotes (5×10^4 cells/well) at a multiplicity of infection (MOI) of 10. After 48 h, infected cells were washed twice with phosphate-buffered saline (PBS) to remove non-internalized parasites and 200 μL of fresh medium was added in duplicate with serial dilution (100 - 1.56 μM) of the Au complexes and BZ. After 72 h, viability of amastigotes was assessed from 50 μL of PBS containing 2 % of Triton X-100 and 200 μM CPRG. β-Galactosidase enzyme catalyzes the hydrolysis of the yellow reagent of CPRG into a red chromophore that is easily detected by an absorbance at 570 nm after 4 h at 37 °C of incubation (microplate reader - Synergy™ H1).[27] Percentage inhibition of 50 % (IC50) on amastigote forms was calculated by a dose-response curve regarding the untreated control.

Cytotoxicity on mammalian cells. The cytotoxicity effects of the Au complexes on LLC-MK2 was asserted by the Thiazolyl Blue Tetrazolium Bromide salt (MTT) as described previously.[38] Mammalian cells were seeded into 96-well plates at a concentration of 5×10^3 cells/well during 48 h at 37 °C and 5 % CO_2. Thereafter, the plates were washed twice with PBS and 200 μL of fresh medium was added in duplicate with serial dilution of the Au complexes and BZ as described above (starting from 100 μM). After 72 h of incubation, the supernatant was carefully removed and 50 μL of MTT solution (2.0 mg/mL) was added on each well. The plates were further incubated for 4 h at 37 °C and the formazan crystals formed were dissolved with DMSO (50 μL/well) after 30 min of incubation at 37 °C. The absorbance data were obtained from a Synergy H1 microplate reader and the cytotoxic concentration of 50 % (CC_{50}) on mammalian cells was calculated by a dose-response curve with regard to the untreated control.

Statistical analysis. *In vitro* data were expressed as mean and standard deviation (S.D.) of three independent experiments performed on three different days. Statistical analysis was performed using one-way analysis of variance (ANOVA) followed by Dunnett's multiple comparison tests. All analyses were made by GraphPad Prism, V5.0 software (GraphPad Software, San Diego, CA, USA) and p-Values < 0.05 were considered as statistically significant.

Acknowledgments

This work was generously supported by the Graduate School (GK 1582) "Fluorine as a key element" of the Deutsche Forschungsgemeinschaft. The authors also would like to thank "Conselho Nacional de Pesquisa" (CNPq) for financial support in Brazil.

Keywords: Thiosemicarbazones · Gold(III) · Chaga's disease · Trypanosoma cruzi · Fluorinated ligands

[1] R. L. Tarleton, *Trends Mol. Med.* **2016**, *22*, 835–838.
[2] J. Bermudez, C. Davies, A. Simonazzi, J. P. Real, S. Palma, *Acta Trop.* **2016**, *156*, 1–16.
[3] J. A. Urbina, R. Docampo, *Trends Parasitol.* **2003**, *19*, 495–501.
[4] P. I. da S. Maia, V. M. Deflon, U. Abram, *Future Med. Chem.* **2014**, *6*, 1515–1536.
[5] P. I. da S. Maia, Z. A. Carneiro, C. D. Lopes, C. G. Oliveira, J. S. Silva, S. de Albuquerque, A. Hagenbach, R. Gust, V. M. Deflon, U. Abram, *Dalton Trans.* **2017**, *46*, 2559–2571.

[6] Y. Zhou, J. Wang, Z. Gu, S. Wang, W. Zhu, J. L. Aceña, V. A. Soloshonok, K. Izawa, H. Liu, *Chem. Rev.* **2016**, *116*, 422–518.
[7] S. W. Chang, A. R. Lewis, K. E. Prosser, J. R. Thompson, M. Gladkikh, M. B. Bally, J. J. Warren, C. J. Walsby, *Inorg. Chem.* **2016**, *55*, 4850–4863.
[8] F. Salsi, G. B. Portapilla, S. Simon, M. Roca Jungfer, A. Hagenbach, S. de Albuquerque, U. Abram, *Inorg. Chem.* **2019**, *58*, 10129–10138.
[9] F. Salsi, G. B. Portapilla, K. Schutjajew, Z. A. Carneiro, A. Hagenbach, S. de Albuquerque, P. I. da S. Maia, U. Abram, *J. Fluorine Chem.* **2018**, *215*, 52–61.
[10] A. Bondi, *J. Phys. Chem.* **1964**, *68*, 441–451.
[11] M. Mantina, A. C. Chamberlin, R. Valero, C. J. Cramer, D. G. Trular, *J. Phys. Chem. A* **2009**, *113*, 7384–7391.
[12] H. Schmidbauer, H. G. Raubenheimer, L. Dobrzanska, *Chem. Soc. Rev.* **2014**, *43*, 345–380.
[13] P. I. da S. Maia, H. H. Nguyen, D. Ponader, A. Hagenbach, S. Bergemann, R. Gust, V. M. Deflon, U. Abram, *Inorg. Chem.* **2012**, *51*, 1604–1613.
[14] A. Rassi, J. Marcondes de Rezende, *Infect. Dis. Clin. North Am.* **2012**, *26*, 275–291.
[15] J. A. Perez-Molina, I. Molina, *Lancet* **2018**, *391*, 82–94.
[16] L. G. Ferreira, A. D. Andricopulo, *Pharmacol. Ther.* **2017**, *180*, 49–61.
[17] A. Casini, C. Hartinger, C. Gabbiani, E. Mini, P. J. Dyson, B. K. Keppler, L. Messori, *J. Inorg. Biochem.* **2008**, *102*, 564–575.
[18] L. Massai, L. Messori, N. Micale, T. Schirmeister, L. Maes, D. Fregona, M. A. Cinellu, C. Gabbiani, *Biometals* **2017**, *30*, 313–320.
[19] J. W. Espindola, M. V. Cardoso, G. B. Filho, E. S. D. A. Oliveira, D. R. Moreira, T. M. Bastos, C. A. Simone, M. B. Soares, F. S. Villela, R. S. Ferreira, M. C. Castro, V. R. Pereira, S. M. Murta, P. A. Sales Junior, A. J. Romanha, A. C. Leite, *Eur. J. Med. Chem.* **2015**, *101*, 818–835.
[20] D. C. Greenbaum, Z. Mackey, E. Hansell, P. Doyle, J. Gut, C. R. Caffrey, J. Lehrman, P. J. Rosenthal, J. H. McKerrow, K. Chibale, *J. Med. Chem.* **2004**, *47*, 3212–3219.
[21] M. C. Fernandes, N. W. Andrews, *Fems Microbiol. Rev.* **2012**, *36*, 734–747.
[22] C. D. Lopes, B. Possato, A. P. S. Gaspari, R. J. Oliveira, U. Abram, J. P. A. Almeida, F. dos Reis Rocho, A. Leitão, C. A. Montanari, P. I. S. Maia, J. S. da Silva, S. de Albuquerque, Z. A. Carneiro, *ACS Infect. Dis.* **2019**, DOI: https://doi.org/10.1021/acsinfecdis.8b00284.
[23] K. M. Bonney, D. J. Luthringer, S. A. Kim, N. J. Garg, D. M. Engman, *Ann. Rev. Pathol.* **2018**, *14*, 421–447.
[24] A. R. L. Teixeira, M. M. Hecht, M. C. Guimaro, A. O. Sousa, N. Nitz, *Clinical. Microbiol. Rev.* **2011**, *24*, 592–630.
[25] E. Chatelain, *J. Biomol. Screening* **2015**, *20*, 22–35.
[26] C. M. Che, R. W. Sun, *Chem. Commun.* **2011**, *47*, 9554–9560.
[27] J. Wang, M. Sanchez-Rosello, J. L. Acena, C. del Pozo, A. E. Sorochinsky, S. Fustero, V. A. Soloshonok, H. Liu, *Chem. Rev.* **2014**, *114*, 2432–2506.
[28] J. Mack, K. Ortner, U. Abram, *Z. Anorg. Allg. Chem.* **1997**, *623*, 873–879.
[29] G. M. Sheldrick, *SADABS*, University Göttingen, Germany, **2014**.
[30] *X-RED32*, An X-ray Data Reduction Tool, STOE & Cie GmbH: Darmstadt, Germany, **2002**.
[31] G. M. Sheldrick, *Acta Crystallogr., Sect. A* **2008**, *64*, 112–122.
[32] G. M. Sheldrick, *Acta Crystallogr., Sect. C* **2015**, *71*, 3–8.
[33] K. Brandenburg, *Diamond-Crystal and Molecular Structure Visualization*, Crystal Impact GbR, Vers. 4.5.1, **2018** Bonn (Germany).
[34] F. S. Buckner, C. Verlinde, A. C. La Flamme, W. C. van Voorhis, *Antimicrob. Agents Chemother.* **1996**, *40*, 2592–2597.
[35] E. P. Camargo, Revista do Instituto de Medicina Tropical de Sao Paulo, **1964**, *6*, 93–100.
[36] M. Rolon, C. Vega, J. A. Escario, A. Gomez-Barrio, *Parasitol. Res.* **2006**, *99*, 103–107.
[37] E. Izumi, T. Ueda-Nakamura, V. F. Veiga, A. C. Pinto, C. V. Nakamura, *J. Med. Chem.* **2012**, *55*, 2994–3001.
[38] T. Mosmann, *J. Immunol. Methods* **1983**, *65*, 55–63.

Received: August 23, 2019